Electronic Coherence in Mixed-Valence Systems: Spectral Analysis

Younjoon Jung, Robert J. Silbey, and Jianshu Cao*

Department of Chemistry, Massachusetts Institute of Technology, Cambridge, Massachusetts 01239

Received: June 1, 1999; In Final Form: August 24, 1999

The electron transfer kinetics of mixed-valence systems is studied via solving the eigenstructure of the two-state nonadiabatic diffusion operator for a wide range of electronic coupling constants and energy bias constants. The calculated spectral structure consists of three branches in the eigendiagram: a real branch corresponding to exponential or multiexponential decay, and two symmetric branches corresponding to population oscillations between donor and acceptor states. The observed electronic coherence is shown as a result of underdamped Rabi oscillations in an overdamped solvent environment. The time evolution of electron population is calculated by applying the propagator constructed from the eigensolution to the nonequilibrium initial preparation, and it agrees perfectly with the result of a direct numerical propagation of the density matrix. The resulting population dynamics confirms that increasing the energy bias destroys electronic coherence.

I. Introduction

Quantum coherence in the dynamics of condensed phase systems has become a subject of recent experimental and theoretical studies. A central issue is the observability of electronic coherence in electron transfer systems given the fast dephasing time in many-body quantum systems. Experimentally, with the advance in ultrafast laser technology, oscillations in electronic dynamics have been observed in photosynthetic reaction centers and other electron transfer systems and are believed to arise from vibrational and/or electronic coherence.[1−3] Accurate measurements on photoinduced electron transfer in mixed-valence compounds have demonstrated oscillations in electronic populations on the femtosecond time scale.[4] Theoretically, detailed path-integral simulations suggest that such oscillations take place in electron transfer systems with large electronic coupling constants and are sensitive to the initial preparation of the bath modes associated with the transfer processes. Lucke et al.[5] extended the noninteracting blip approximation to incorporate the nonequilibrium initial preparation and carried out extensive path-integral quantum dynamics simulations for electron transfer reactions. According to their findings, large-amplitude oscillations are most likely to be observed in symmetric mixed-valence systems that are nearly adiabatic and with initial configurations that are centered in the Landau−Zener crossing region. Using the transfer matrix technique,[6] Evans, Nitzan, and Ratner[7] calculated short-time evolution for the photoinduced electron transfer reaction in $(NH_3)_5Fe^{II}(CN)Ru^{III}(CN)_5$. Their results show fast oscillations in the electronic population on the short time scale (20 fs) followed by a slower population relaxation on the long time scale (100 fs). They pointed out that these fast oscillations arise as the wave function oscillates coherently between the donor and acceptor states. The calculated long-time decay rate is considerably smaller than the prediction by the golden-rule formulas,[8,9] confirming the inadequacy of nonadiabatic rate theory in studying mixed-valence systems.

In fact, a simple classical argument helps understand the nature of the observed oscillations. As a function of the ratio between λ (the bath reorganization energy) and V (the electronic coupling constant), there is a thermodynamic transition from the localized electronic state in a double-well potential to the delocalized electronic state in a single-well potential.[10−14] (i) In the localized regime ($\lambda \gg V$), the large reorganization energy destroys electronic coherence; hence, electron transfer is an incoherent rate process, which can be described by the noninteracting blip approximation or golden-rule rate in the nonadiabatic limit and by transition state theory in the adiabatic limit.[15−17] (ii) In the delocalized regime ($\lambda \leq V$), the electronic wave function extends to both the donor and acceptor states and electronic coherence persists over several oscillations.[10] For mixed-valence compounds, the electronic coupling constant is estimated to be in the range of 10^3 cm^{-1}, which is in the same order as the reorganization energy.[1,7] Therefore, the observed oscillations and relaxation in mixed-valence systems are the consequence of a highly nonequilibrium coherence transfer process.

Due to the delocalization nature of electronic states, an adiabatic picture[18] is more useful than the diabatic representation for analyzing the short-time dynamics in strongly-coupled systems. In this picture, electronic coherence arises from Rabi oscillations between two adiabatic surfaces and decays because of electronic dephasing. Further, initial preparation and wave-packet dynamics can modulate Rabi oscillations and the overall electronic dynamics. Thus, the adiabatic representation provides a simple picture for mixed-valence systems as well as a simple analytical method to model fast electron dynamics initiated by laser pulses.

As a general approach to describe condensed phase dynamics, we recently proposed a spectral analysis method,[19] which is based on eigenstructures of dissipative systems instead of dynamic trajectories. An important application of the approach is to analyze a set of two-state diffusion equations, which was first used by Zusman to treat solvent effects on electron transfer in the nonadiabatic limit. The analysis allows us to characterize multiple time scales in electron transfer processes including vibrational relaxation, electronic coherence, activated curve crossing, or barrier crossing. With this unified approach, the observed rate behavior, biexponential and multiexponential decay, and population oscillations are different components of the same kinetic spectrum. Thus, several existing theoretical

---

* Corresponding author. E-mail: jianshu@mit.edu.

10.1021/jp9917594 CCC: $18.00

models, developed for limited cases of electron transfer, can be analyzed, tested, and extended. In particular, rate constants extracted from the analysis bridge smoothly between the adiabatic and nonadiabatic limits, and the kinetic spectrum in the large coupling regime reveals the nature of the localization−delocalization transition as the consequence of two competing mechanisms.

In this paper, the spectral analysis approach developed in ref 19 is employed to study the electron transfer dynamics in mixed-valence systems. We invoke the nonadiabatic diffusion equation proposed by Zusman to describe the electron transfer process in the over-damped solvent regime. As discussed earlier, electron transfer in mixed-valence systems takes place in a different kinetic regime from the thermal activated regime described by Marcus theory. Thus, the time-scale separation is not satisfied, and multiexponential decay and oscillations are intrinsic nature of electron transfer kinetics. As a result, the kinetic spectra exhibit bifurcation, coalescence, and other complicated patterns. Careful examination of these patterns reveals the underlying mechanisms in mixed-valence systems.

The rest of the paper is organized as follows: The spectral structure of the nonadiabatic diffusion equation is formulated in section II. Numerical examples of the spectral structure of strongly mixed electron transfer systems are presented and discussed in section III, and concluding remarks are given in section IV.

II. Theory

There have been extensive studies of the solvent effect on electron transfer dynamics in literature with various approaches.[20−24] One of the most extensively studied models for quantum dissipation is the spin−boson Hamiltonian,[14,23]

$$H_{\mathrm{SB}} = \frac{\epsilon}{2}\sigma_z + V\sigma_x + \sum_\alpha \frac{p_\alpha{}^2}{2m_\alpha} + \sum_\alpha \frac{1}{2} m_\alpha \omega_\alpha^2 \left(x_\alpha - \sigma_z \frac{c_\alpha}{m_\alpha \omega_\alpha{}^2} \right)^2 \tag{1}$$

where ϵ is the energy bias between the two electronic states, V is the electronic coupling constant, σ_z and σ_x are the usual Pauli matrices, and $\{x_\alpha, p_\alpha\}$ represents the bath degree of freedom with mass m_α, frequency ω_α, and the coupling constant c_α. In this model effects of the bath modes on the dynamics of the system can be described via the spectral density defined by

$$J(\omega) = \frac{\pi}{2} \sum_\alpha \frac{c_\alpha{}^2}{m_\alpha \omega_\alpha} \delta(\omega - \omega_\alpha) \tag{2}$$

Equivalently, the spin−boson Hamiltonian in eq 1 can be separated into the electronic two-level part H_{TLS} and the nuclear bath part H_{B},

$$H_{\mathrm{SB}} = H_{\mathrm{TLS}} + H_{\mathrm{B}} \tag{3}$$

The two-level part of the Hamiltonian can be explicitly written as

$$H_{\mathrm{TLS}}(E) = U_1(E)|1\rangle\langle 1| + U_2(E)|2\rangle\langle 2| + V(|1\rangle\langle 2| + |2\rangle\langle 1|) \tag{4}$$

where the diabatic energy surfaces $U_1(E)$ and $U_2(E)$ are functions of the stochastic variable E, which represents the polarization energy for a given solvent configuration.[20] The transformation from the spin−boson Hamiltonian to the two-level system Hamiltonian has been shown in the literature[23,25] by the identity

$$E(\{x_\alpha\}) = \sum_\alpha c_\alpha x_\alpha \tag{5}$$

It is worthwhile to mention that the polarization energy E was recognized as the reaction coordinate by Marcus in formulating nonadiabatic electron transfer theory.[15] Since the electron transfer process involves the collective motion of a large number of solvent degrees of freedom and the two-level system is linearly coupled to the harmonic bath modes in the spin−boson Hamiltonian in eq 1, the functional form for the free energy surface is harmonic,[26] thus giving

$$U_1(E) = \frac{(E+\lambda)^2}{4\lambda} \tag{6}$$

$$U_2(E) = \frac{(E-\lambda)^2}{4\lambda} + \epsilon \tag{7}$$

where λ is the reorganization energy, which is related to the parameters in eq 1

$$\lambda = \sum_\alpha \frac{c_\alpha{}^2}{2m_\alpha \omega_\alpha{}^2} = \frac{1}{\pi} \int \mathrm{d}\omega \frac{J(\omega)}{\omega} \tag{8}$$

Considering the fact that electron transfer processes are usually probed at room temperature in polar solvents, we can treat the bath degrees of freedom in H_{B} classically. Then, the spin−boson Hamiltonian in eq 3 can be used to derive a two-level classical equation of motion

$$i\frac{\partial}{\partial t}\rho(t) = \mathsf{L}\rho(t) + (\mathsf{L}_{\mathrm{B}} + \mathsf{L}_{\mathrm{TLS}})\rho(t) \tag{9}$$

where $i\mathsf{L}_{\mathrm{B}} = \{\ , H_{\mathrm{B}}\}$ is the Poisson operator for the classical bath and $\mathsf{L}_{\mathrm{TLS}} = [H_{\mathrm{TLS}},]/\hbar$ is the Liouville operator for the two-level system. Explicitly, we express eq 9 in terms of the density matrix elements

$$\dot{\rho}_1 = \mathsf{L}_1\rho_1 + iV(\rho_{12} - \rho_{21}) \tag{10a}$$

$$\dot{\rho}_2 = \mathsf{L}_2\rho_2 - iV(\rho_{12} - \rho_{21}) \tag{10b}$$

$$\dot{\rho}_{12} = \mathsf{L}_{12}\rho_{12} - i\omega_{12}\rho_{12} + iV(\rho_1 - \rho_2) \tag{10c}$$

$$\dot{\rho}_{21} = \mathsf{L}_{21}\rho_{21} + i\omega_{12}\rho_{21} - iV(\rho_1 - \rho_2) \tag{10d}$$

where the Planck constant $\hbar$ is set to unity for simplicity, ρ_i is the diagonal matrix element for electronic population, and ρ_{ij} is the off-diagonal matrix element for electronic coherence. Here, L describes the relaxation process of classical bath, with L_i defined on the free energy surface for the ith electronic state, and with L_{12} and L_{21} defined on the averaged free energy surface. This set of semiclassical two-state equations has been previously derived in different context by several authors.[20,23,27] It should be mentioned that the mapping from the spin−boson Hamiltonian into the Zusman model requires the Lorentzian form of the spectral density

$$J(\omega) = 2\lambda \frac{\omega\omega_{\mathrm{c}}}{\omega^2 + \omega_{\mathrm{c}}{}^2} \tag{11}$$

Furthermore, we note that many chemically and biologically important electron transfer processes take place in the overdamped solvent environment. Therefore, to describe the density matrix evolution in the electron transfer kinetics in the mixed-valence system, we invoke the nonadiabatic diffusion equation proposed by Zusman.[20] Then, the bath relaxation operators in eq 9 are one-dimensional Fokker−Planck operators $\mathcal{L}_{ij}$

$$\mathcal{L}_i = D_{\mathrm{E}} \frac{\partial}{\partial E}\left(\frac{\partial}{\partial E} + \beta \frac{\partial U_{\mathrm{i}}(E)}{\partial E}\right) \tag{12}$$

$$\mathcal{L}_{12} = \mathcal{L}_{21} = \frac{\mathcal{L}_{11} + \mathcal{L}_{22}}{2} = D_{\mathrm{E}} \frac{\partial}{\partial E}\left(\frac{\partial}{\partial E} + \beta \frac{\partial \bar{U}(E)}{\partial E}\right) \tag{13}$$

where $\beta = 1/k_{\mathrm{B}}T$, $\bar{U}$ and ω_{12} are the average and the difference of the two free energy surfaces, respectively

$$\bar{U}(E) = \frac{U_1(E) + U_2(E)}{2} \tag{14}$$

$$\omega_{12}(E) = U_1(E) - U_2(E) \tag{15}$$

The energy diffusion constant D_{E} is defined as

$$D_{\mathrm{E}} = \Omega {\Delta_{\mathrm{E}}}^2 \tag{16}$$

where Δ_E^2 is the mean square fluctuation of the solvent polarization energy

$$\Delta_E^{\;2} = \langle E^2 \rangle = 2\lambda k_{\mathrm{B}} T$$

and $\tau_{\mathrm{D}} = 1/\Omega$ is the the characteristic timescale of the Debye solvent. The correlation function of the solvent polarization energy is given by

$$C(t) = \langle E(t)\, E(0) \rangle = \Delta_E^{\;2} \exp(-\Omega t) \tag{17}$$

Note that since the nuclear dynamics is modeled by the Fokker−Planck operator, the possibility of the vibrational coherence is excluded in this model of electron transfer dynamics. It is worthwhile to mention that one can obtain the nonadiabatic diffusion equation starting from the spin−boson Hamiltonian by first deriving the evolution equation for the quantum dissipative dynamics, and then taking the semiclassical limit using the Wigner distribution functions, and finally assuming the overdamped diffusion limit.[23]

We investigate the spectral structure of the nonadiabatic diffusion operator by calculating the eigenvalues $\{-Z_\nu\}$ and the corresponding eigenfunctions $\{|\psi_\nu\rangle\}$. Hereafter we use Greek indices to denote the eigenstates and Latin indices to denote the basis states of the nonadiabatic diffusion operator. Because the nonadiabatic Liouville operator is non-Hermitian, the eigenvalues are generally given by complex values, and the right and left eigenfunctions corresponding to the same eigenvalue are not simply the Hermitian conjugate to each other.[28] For a given eigenvalue Z_ν, the right and left eigenfunctions of the nonadiabatic diffusion operator are obtained from

$$\mathcal{L}\, |\psi_\nu^{\mathrm{R}}\rangle = -Z_\nu |\psi_\nu^{\mathrm{R}}\rangle \tag{18}$$

$$\langle \psi_\nu^{\mathrm{L}} | \mathcal{L} = -Z_\nu \langle \psi_\nu^{\mathrm{L}} | \tag{19}$$

The method of eigenfunction solution is well-known for the diffusion process on the harmonic potential energy surface.[29] For a single quadratic potential $U(x) = {}^1/_2 m\omega^2 x^2$, the one-dimensional Fokker−Planck operator $\mathcal{L}_{\mathrm{FP}} = D((\partial^2/\partial x^2) + \beta\partial U'/\partial x)$ can be transformed into the quantum mechanical Hamiltonian in imaginary time

$$H_{\mathrm{s}} = -\mathrm{e}^{\beta U(x)/2} \mathcal{L}_{\mathrm{FP}} \mathrm{e}^{-\beta U(x)/2} = -\frac{1}{2\mu}\frac{\partial^2}{\partial x^2} + V_{\mathrm{s}}(x) \tag{20}$$

where $\mu^{-1} = 2D$, and the quadratic potential is

$$V_{\mathrm{s}}(x) = D\left[\frac{1}{4}(\beta U'(x))^2 - \frac{1}{2}\beta U''(x)\right] = \frac{1}{2}\mu\gamma^2 x^2 - \frac{\gamma}{2} \tag{21}$$

with $\gamma = Dm\omega^2/k_{\mathrm{B}}T$. Since the transformed potential in eq 21 is just the same form as for a simple harmonic oscillator with zero-point energy compensation, the eigenvalues and the eigenfunctions for the original Fokker−Planck operator can be constructed immediately from the eigensolutions of the harmonic oscillator Hamiltonian. Unlike the diffusion problem on the single potential energy surface, there have been limited studies on the nonadiabatic diffusion problem involving more than one potential energy surface. In this aspect, Cukier and co-workers have calculated the electron transfer rate by calculating the lowest eigenvalue of the nonadiabatic diffusion equation; however, their calculation was limited to the weak-coupling regime where the Zusman rate is applicable.[27]

An important issue in solving the nonadiabatic diffusion equation for electron transfer is the choice of the basis functions since three different free energy surfaces are involved in eq 9: two diabatic surfaces for the population density matrix elements and one averaged surface for the coherence density matrix element. In this paper, the eigenfunctions of $\mathcal{L}_{12}$ are used as our basis set to represent the nonadiabatic diffusion equation. In principle, one could have chosen the eigenfunctions of $\mathcal{L}_1$ or $\mathcal{L}_2$ as basis functions; however, in that case one has to evaluate appropriate Franck−Condon factors when calculating the coupling matrix elements even with the Condon approximation. The Fokker−Planck operator $\mathcal{L}_{12}$ is defined on the averaged harmonic potential centered at $E = 0$, and its eigensolutions are

$$\mathcal{L}_{12} |\phi_n^{\mathrm{R}}\rangle = -n\Omega |\phi_n^{\mathrm{R}}\rangle \tag{22}$$

$$\langle \phi_n^{\mathrm{L}} | \mathcal{L}_{12} = -n\Omega \langle \phi_n^{\mathrm{L}} | \tag{23}$$

where the right and left eigenfunctions are

$$\phi_n^{\mathrm{R}}(E) = \frac{1}{(2^n n!)^{1/2} (2\pi \Delta_E^{\;2})^{1/4}} \exp\left(-\frac{E^2}{2\Delta_E^{\;2}}\right) H_n\left(\frac{E}{\sqrt{2}\Delta_E}\right) \tag{24}$$

$$\phi_n^{\mathrm{L}}(E) = \frac{1}{(2^n n!)^{1/2} (2\pi \Delta_E^{\;2})^{1/4}} H_n\left(\frac{E}{\sqrt{2}\Delta_E}\right) \tag{25}$$

where H_n is the nth-order Hermite polynomial. As shown below, this choice of the basis set is convenient for our purpose.

To be consistent with the $\mathcal{L}_{12}$ basis set, we separate the real and imaginary parts of the coherence density matrix, namely, $u = \mathrm{Re}\rho_{12}$ and $v = \mathrm{Im}\rho_{12}$, and rewrite eq 9 as

$$\dot{\rho}_1 = (\mathcal{L}_{12} + \delta\mathcal{L}\,)\rho_1 - 2Vv \tag{26a}$$

$$\dot{\rho}_2 = (\mathcal{L}_{12} - \delta\mathcal{L}\,)\rho_2 + 2Vv \tag{26b}$$

$$\dot{u} = \mathcal{L}_{12} u + \omega_{12} v \tag{26c}$$

$$\dot{v} = \mathcal{L}_{12} v - \omega_{12} u + V(\rho_1 - \rho_2) \tag{26d}$$

where we have defined δL as

$$\delta L = \frac{L_{11} - L_{22}}{2} \tag{27}$$

Then, all the relevant operators in eqs 26a−26d can be evaluated in terms of the right and left eigenfunctions of L_{12}, giving

$$\langle \phi_n^{\mathrm{L}} | L_{12} | \phi_m^{\mathrm{R}} \rangle = -n\Omega\delta_{nm} \tag{28}$$

$$\langle \phi_n^{\mathrm{L}} | \delta L | \phi_m^{\mathrm{R}} \rangle = -\Omega\sqrt{\frac{\lambda}{2k_{\mathrm{B}}T}}\sqrt{m+1}\,\delta_{n,m+1} \tag{29}$$

$$\langle \phi_n^{\mathrm{L}} | \omega_{12} | \phi_m^{\mathrm{R}} \rangle = \sqrt{2\lambda k_{\mathrm{B}}T}(\sqrt{m}\,\delta_{n,m-1} + \sqrt{m+1}\,\delta_{n,m+1}) - \epsilon\delta_{nm} \tag{30}$$

$$\langle \phi_n^{\mathrm{L}} | V | \phi_m^{\mathrm{R}} \rangle = V\delta_{nm} \tag{31}$$

where we assume the Condon approximation; i.e., the electronic coupling matrix element is independent of the solvent degrees of freedom. With the basis set, we can expand the density matrix elements as

$$\rho_1(E,t) = \sum_{n=0}^{\infty} a_n(t)\phi_n^{\mathrm{R}}(E) \tag{32a}$$

$$\rho_2(E,t) = \sum_{n=0}^{\infty} b_n(t)\phi_n^{\mathrm{R}}(E) \tag{32b}$$

$$u(E,t) = \sum_{n=0}^{\infty} c_n(t)\phi_n^{\mathrm{R}}(E) \tag{32c}$$

$$v(E,t) = \sum_{n=0}^{\infty} d_n(t)\phi_n^{\mathrm{R}}(E) \tag{32d}$$

Substituting eqs 32a−32d into the eigenvalue equation eq 18, we have the following coupled linear equations

$$-Z_\nu a_n = -n\Omega a_n - \Omega\sqrt{\frac{\lambda}{2k_{\mathrm{B}}T}}\sqrt{n}\,a_{n-1} - 2Vd_n \tag{33a}$$

$$-Z_\nu b_n = -n\Omega b_n + \Omega\sqrt{\frac{\lambda}{2k_{\mathrm{B}}T}}\sqrt{n}\,b_{n-1} + 2Vd_n \tag{33b}$$

$$-Z_\nu c_n = -n\Omega c_n + \sqrt{2\lambda k_{\mathrm{B}}T}(\sqrt{n+1}\,d_{n+1} + \sqrt{n}\,d_{n-1}) - \epsilon d_n \tag{33c}$$

$$-Z_\nu d_n = -n\Omega d_n - \sqrt{2\lambda k_{\mathrm{B}}T}(\sqrt{n+1}\,c_{n+1} + \sqrt{n}\,c_{n-1}) + \epsilon c_n + V(a_n - b_n) \tag{33d}$$

which is an explicit basis set representation for the two-state diffusion operator in eq 9. The linear equations for the left eigensolution as defined by eq 19 can be written by the transpose of eqs 33a−33d. Diagonalizing the $4N \times 4N$ matrix (N = number of basis functions) defined in eqs 33a−33d, we obtain the eigenvalues $-Z_\nu$ and the corresponding eigenvectors of the nonadiabatic diffusion operator

$$|\psi_\nu^{\mathrm{R}}\rangle = \sum_n R_{n\nu}|\phi_n^{\mathrm{R}}\rangle \tag{34}$$

$$\langle\psi_\nu^{\mathrm{L}}| = \sum_n L_{\nu n}\langle\phi_n^{\mathrm{L}}| \tag{35}$$

where $R_{n\nu}$ and $L_{\nu n}$ are elements of the transformation matrices.

In general, due to the non-Hermitian nature of the nonadiabatic diffusion operator, the right and left eigenfunctions do not form an orthogonal set by themselves. However, when the eigenvalues are all nondegenerate, the left and right eigenfunctions form an orthogonal and complete set in dual Hilbert space.[30] Explicitly, we have

$$\sum_{n=0} L_{\nu n}R_{n\nu'} = \delta_{\nu\nu'} \tag{36}$$

for the orthogonality and

$$\sum_\nu R_{n\nu}L_{\nu n} = \delta_{nm} \tag{37}$$

for the completeness. Using these properties, we can construct the real time propagator for the operator L as

$$G(t) = \sum_\nu |\psi_\nu^{\mathrm{R}}\rangle\langle\psi_\nu^{\mathrm{L}}|\mathrm{e}^{-Z_\nu t} \tag{38}$$

and express the time evolution of the density matrix by projecting a given initial distribution onto the eigenstates, giving

$$|\rho(t)\rangle = G(t)|\rho(0)\rangle = \sum_\nu |\psi_\nu^{\mathrm{R}}\rangle\langle\psi_\nu^{\mathrm{L}}|\rho(0)\rangle\mathrm{e}^{-Z_\nu t} \tag{39}$$

Hence, the eigensolution to the two-state nonadiabatic diffusion equation leads to a complete description of electron transfer dynamics.

III. Results and Discussion

In the section, we present the spectral structure of the nonadiabatic diffusion operator by diagonalizing its matrix representation in eqs 33a−33d. In principle, we need infinite number of basis functions to diagonalize the nonadiabatic diffusion operator; however, in practice, we have to truncate our basis set at some finite number. In all the calculations below, we have used N = 50−200 to diagonalize the $4N \times 4N$ matrix and the effect of finite number basis on the spectral structure has been carefully examined.

A. Spectral Structure. *1. Mixed-Valence Systems.* In the mixed-valence compounds, the electronic coupling constant has the same order of magnitude as the reorganization energy and the electron transfer dynamics is usually probed experimentally at room temperature in polar solvents. To study this process, Evans, Nitzan, and Ratner[7] carried out real time path-integral simulations for the photoinduced electron transfer reaction in $(NH_3)_5Fe^{II}(CN)Ru^{III}(CN)_5$. On the basis of their model, we chose the parameters for the calculation shown in Figure 1 as $\beta\Omega$ = 0.6716, $\beta\lambda$ = 18.225, βV = 11.99, and $\beta\epsilon$ = 18.705. As mentioned in the Introduction, the mapping between the spin−boson Hamiltonian and the semiclassical Zusman equation is not rigorously defined. For example, for the nonadiabatic diffusion equation, the solvation energy correlation function takes an exponential form with the rate Ω, whereas for the spin−boson model Hamiltonian, it depends on the functional form

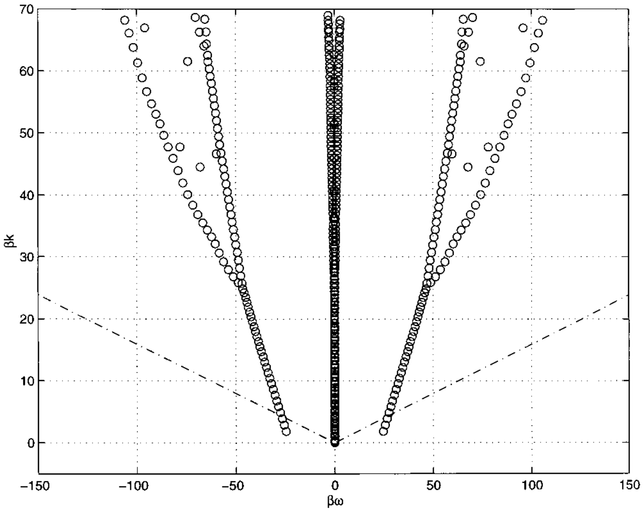

Figure 1. A plot of the lowest 400 eigenvalues for the nonadiabatic operator in a mixed-valence system. The parameters are $\beta\Omega = 0.6716$, $\beta\lambda = 18.225$, $\beta V = 11.99$, and $\beta\epsilon = 18.705$. The dot-dashed line is for the case $k = \omega/2\pi$.

of the spectral density. It can be shown that the Ohmic spectral density with an exponential cutoff ω_c

$$J(\omega) = \eta\omega \exp(-\omega/\omega_c) \qquad (40)$$

used in the calculation of Evans et al. leads to an energy correlation function with a Lorentzian form at high temperature[23]

$$C_{SB}(t) \approx \frac{2\eta\omega_c k_B T}{\pi}\frac{1}{1 + (\omega_c t)^2} \qquad (41)$$

Then, the relaxation rate Ω used in our calculation is taken as the inverse of the mean survival time of $C_{SB}(t)$, which is $\Omega = 2\omega_c/\pi$.

In Figure 1 the spectral structure of the nonadiabatic operator is shown in complex space. We have used $N = 200$ ($4N = 800$) basis functions to calculate the eigenvalues. To remove the effect of finite basis set from the resulting spectral structure, we only show the first 400 eigenvalues in the complex plane. Since the nonadiabatic diffusion operator is non-Hermitian, the resulting spectrum shows complex conjugate paired eigenvalues as well as real eigenvalues, giving rise to the tree structure with three major branches (which we will call the *eigentree*). In Figure 1, we separate the real and imaginary parts of eigenvalue by

$$-Z_\nu = -k_\nu - i\omega_\nu \qquad (42)$$

Obviously, the real part, $-k_\nu$, is always negative as all nonequilibrium physical quantities decay to zero at time infinity, and it scales linearly with the index ν since the relaxation rate corresponding to the nth basis state ϕ_n is proportional to n. In general, the relative magnitudes of real and imaginary parts of eigenvalues determine the time evolution of the density matrix: the real eigenvalues correspond to the simple exponential decay components and the complex conjugate paired eigenvalues correspond to the damped oscillation components.

To classify the eigenvalues quantitatively according to their dynamic behavior, we introduce the dimensionless quantity θ_ν

$$\theta_\nu \equiv \frac{2\pi k_\nu}{|\omega_\nu|} \qquad (43)$$

where k_ν is the decay rate and $2\pi/\omega_\nu$ is the oscillation period. The time evolution of the density matrix component associated with the eigenvalue Z_ν is an exponential decay if $\theta_\nu = \infty$, an underdamped oscillation if $\theta_\nu \leq 1$, and a damped oscillation if $\theta_\nu > 1$. The relative amplitude of each component depends on the overlap matrix element between the initial density matrix and the eigenstate. As an approximate criterion for the classification of the eigenvalues, the slope corresponding to $\theta_\nu = 1$ is shown in the eigentree diagram in Figure 1. There are a few eigenstates around and below the $\theta_\nu = 1$ line, with a typical rate of $\beta k_\nu \approx 5$. For the parameters used in the calculation, β corresponds to ~170 fs in real time, and, therefore, these eigenstates exhibit underdamped oscillations with a period and a decay time in the femtosecond regime. In their real-time path integral simulations, Evans et al. showed that the population in the acceptor state oscillates with a few femtosecond period and these oscillations decay within 20 fs. Thus, qualitative features of the electron transfer dynamics can be predicted and understood from a careful examination of the spectral structure. Since the spectral analysis presented here is based on the semiclassical diffusion equation while the path-integral study is based on the quantum mechanical spin−boson Hamiltonian, the comparison between the two approaches is expected to be qualitative. In the following subsection, further analysis reveals the nature of these oscillations.

2. Dependence on the Coupling Constant V. To examine the underlying spectral structure in more detail, eigenvalues of the nonadiabatic diffusion operator are plotted as functions of the electronic coupling constant in Figure 2. All the parameters except for the electronic coupling constant are the same as used in Figure 1.

In Figure 2a, the real parts of the first 20 eigenvalues are shown as functions of the electronic coupling constant. Note that eigenvalues corresponding to complex conjugate pairs have the same real part, and thus they coalesce in the real eigenvalue diagram. When the coupling constant is very small ($\beta V \ll 1$), the real part of the first nonzero eigenvalue is very well separated from the eigenvalues of excited states, so the dynamics of electron transfer can be considered as a incoherent rate process with a well-defined rate constant, k_1. When the coupling constant is larger ($\beta V \approx 1$), the first excited state becomes close to the second excited state, and they start to merge into a complex conjugate pair. If the coupling constant increases further, eigenvalues show a bifurcation behavior at $\beta V \approx 10$. Therefore, in this regime, the electron transfer kinetics show multiple time scale relaxation as well as coherent oscillation. The complicated behavior of coalescence and bifurcation in the real eigenvalue appears more frequently at higher states.

Another interesting feature of the real eigenvalue diagram is that a set of real eigenvalues decreases consistently as the coupling constant increases from zero. It turns out that these eigenstates take on large imaginary parts, which are responsible for the onset of the imaginary branches of the eigentree. In Figure 2b, the imaginary parts of the lowest 30 eigenvalues are plotted as functions of the coupling constant. Interestingly, the imaginary part of the eigenvalue increases approximately linearly with the coupling constant at large coupling regime. In fact, the dependence on the coupling constant is similar to that of the Rabi frequency for the two-level system

$$\Omega_R = \sqrt{\epsilon^2 + 4V^2} \qquad (44)$$

which is shown in Figure 2b. As pointed out in a recent paper,[18] electronic coherence in mixed-valence systems arises from Rabi

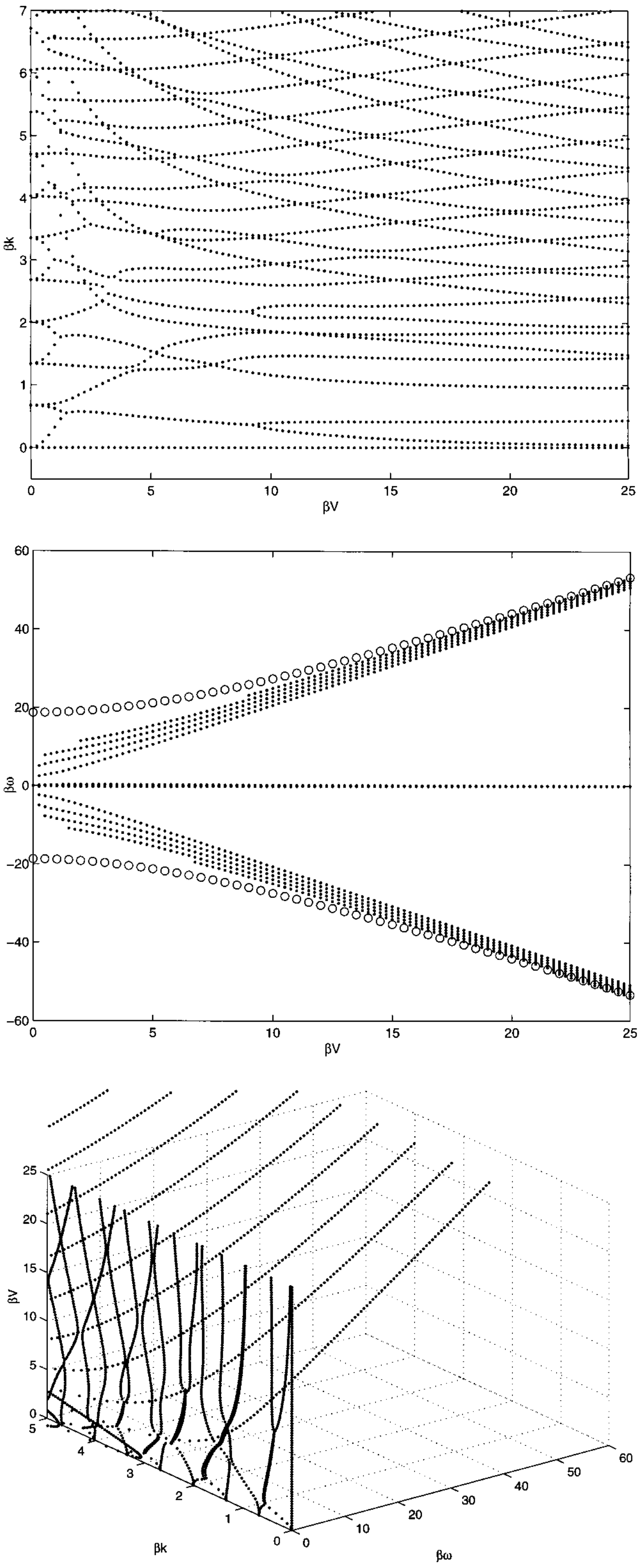

Figure 2. Plots of (a, top) real and (b, middle) imaginary parts of the lowest 30 eigenvalues as a function of the coupling constant, V. Except for the coupling constant, all the other parameters are set equal to those used in Figure 1. In (b), open circles correspond to the Rabi frequency $\Omega_R = (\epsilon^2 + 4V^2)^{1/2}$. (c, bottom) Three-dimensional plot of eigenvalues as a function of the coupling constant.

oscillations between two adiabatic surfaces and decays because of dephasing.

To demonstrate the correlation of the real and imaginary parts of the eigenvalues as functions of the coupling constant, we present a three-dimensional plot of the spectral structure in Figure 2c. For clarity, only the positive branches of the imaginary eigenvalues are shown. If we compare Figure 2c with Figure 2a, the very rapidly decaying states shown in Figure 2a take on large imaginary parts corresponding to the Rabi oscillations as the coupling constant increases, and these states are responsible for the onset of the imaginary branches in the eigentree for the mixed-valence system shown in Figure 1.

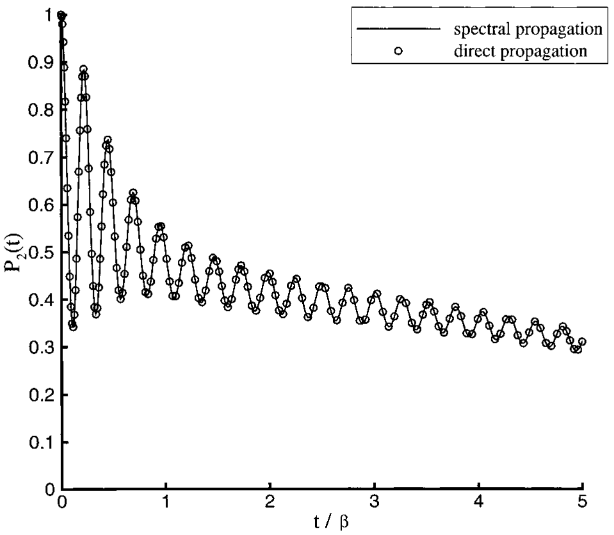

Figure 3. Comparison between the result of direct numerical propagation and spectral propagation. The parameters are chosen as $\beta\Omega = 1$, $\beta\lambda = 15$, $\beta V = 12$, and $\beta\epsilon = 3$.

B. Density Matrix Propagation. To check the validity of the spectral analysis as a density matrix propagation scheme, we calculated the time evolution of the density matrix by applying the propagator defined by eq 38 to the initial density matrix for various energy biases. Although it may seem straightforward to use the spectral method as a propagation scheme, the case for a non-Hermitian operator is not trivial and has not been explored. The main reason is that though the left and right eigenfunctions of a non-Hermitian operator can be shown to form a biorthogonal set for the nondegenerate eigenvalue case, numerically these eigenfunctions may not be stable enough to be used as a complete orthonormal basis for the density matrix propagation, especially in the nearly degenerate eigenvalue case. We can understand the situation as follows: When the two nearly degenerate eigenvalues Z_1 and Z_2 are obtained from a non-Hermitian operator, the orthogonality implies that $\langle L_2|$ and $|R_1\rangle$ are orthogonal to each other as well as $\langle L_1|$ and $|R_2\rangle$. When two eigenvalues become very close to each other, unlike the Hermitian operator case, $\langle L_1|$ and $\langle L_2|$ almost coincide and so do $|R_1\rangle$ and $|R_2\rangle$, so that $\langle L_1|$ and $|R_1\rangle$ become almost orthogonal to each other. To still satisfy the normalization condition $\langle L_n|R_n\rangle$ in this case, the eigenfunction should be scaled up, thus making the spectral structure very sensitive to the numerical error involved in the calculation of eigenfunctions. For an interesting discussion on this point, one may refer to the work by Nelson and co-workers.[30] Due to this numerical instability, the use of the spectral method as a density matrix propagation scheme is not without limitation.

Figure 3a shows the spectral structure and the time evolution of the density matrix propagation for the case of $\beta\Omega = 1$, $\beta\lambda = 15$, $\beta V = 12$, and $\beta\epsilon = 5$. Generally, when the energy bias is small ($\beta\epsilon \le 5$), the left and right eigenfunctions can form a complete orthonormal basis set, so the spectral method is stable and can be used as a numerical propagation method for the density matrix. With a large energy bias, however, the calculated eigenfunctions may not form a complete orthonormal basis. To model for the photoinduced back electron transfer experiment in the mixed-valence compounds the initial density matrix is chosen as a thermal equilibrium distribution of the donor state (i.e., 1-state) pumped to the acceptor state (i.e., 2-state),[4,5,7]

$$\rho_i(E,0) = \frac{1}{\sqrt{2\pi}\Delta_E} \exp\left(-\frac{(E+\lambda)^2}{2\Delta_E^{\,2}}\right)\delta_{i2} \tag{45a}$$

$$\rho_{12}(E,0) = \rho_{21}(E,0) = 0 \tag{45b}$$

It would be straightforward to calculate the spatial distribution of the density matrix in time $\rho(E,t)$ by applying the propagator in eq 38 to the above initial density matrix; however, to demonstrate the overall temporal behavior only the time evolution of the total population in the acceptor state is calculated

$$P_2(t) = \int \mathrm{d}E\ \rho_2(E,t) \tag{46}$$

In order to check the validity of the spectral method as a propagation scheme in this case, we also calculated the time evolution of the density matrix by directly solving the 4*N* differential equations for the expansion coefficients of the density matrix using the Bulirsh−Stoer algorithm,[31] and the comparison in Figure 3a shows a perfect agreement. If only the transient behavior is concerned with, the direct propagation method would be preferred over the spectral method; however, the spectral propagation has the advantage when calculating the long-time behavior once the complete spectrum is known. Overall, the computational costs for the two methods are comparable to each other. As expected from the spectral structure shown in the previous section, the population in the acceptor state shows an underdamped coherent oscillation behavior at initial times followed by a damped oscillation behavior at later times.

Further, we have also studied the density matrix propagation for different energy biases to examine the electronic dephasing effect. As seen from Figure 4a, the increase in energy bias destroys the electronic coherence dramatically. Another interesting observation is the phase shift in the population dynamics as the energy bias is varied, and it is because the Rabi oscillation frequency increases with energy bias. We can confirm the temporal behavior of the density matrix propagation by examining the spectral structure shown in Figure 4b. The period of the initial coherence is estimated to be $\tau_{\rm osc} \approx 0.25\beta$ from Figure 4a. In comparison, the Rabi frequency for the corresponding adiabatic two-level system is given by $\Omega_{\rm R} = (\epsilon^2 + 4V^2)^{1/2} \approx 25\beta^{-1}$, which can also be obtained from the onset of imaginary branches in the eigentree shown in Figure 4b, and the estimation is consistent with the oscillation period observed in the dynamics since $\tau_{\rm osc} \approx 2\pi/\Omega_{\rm R}$. The real eigenvalues of the lowest excited states in the the imaginary branches are estimated to be $\beta k \approx 1-2$, and they agree with the decay time of the oscillation amplitude in Figure 4a, confirming the validity of the spectral method as a density matrix propagation scheme. Even though it has been well-known in the literature that the damping of population is enhanced with increased energy asymmetry,[14] we have also confirmed this through the spectral analysis method.

As an example of the eigenfunction responsible for the coherent oscillation behavior observed in Figure 4b, we show the left and right eigenfunctions corresponding to a complex eigenvalue $\beta Z = 2.6228 \pm i26.394$ for a symmetric case ($\beta\epsilon = 0$) and $\beta Z = 2.8057 \pm i26.466$ for an asymmetric case ($\beta\epsilon = 5$) in Figures 5 and 6. The eigenfunctions corresponding to a complex conjugate pair of eigenvalues are also complex conjugate to each other; therefore, the frequency spectrum of the density matrix evolution is proportional to the norm of wave function. We note that the left eigenfunction is more extended than the right eigenfunction. Although the population distribution in the donor and acceptor states corresponding to coherent oscillation is inverted with respect to the Boltzmann distribution, it does not contribute to the steady-state population distribution due to the transient nature.

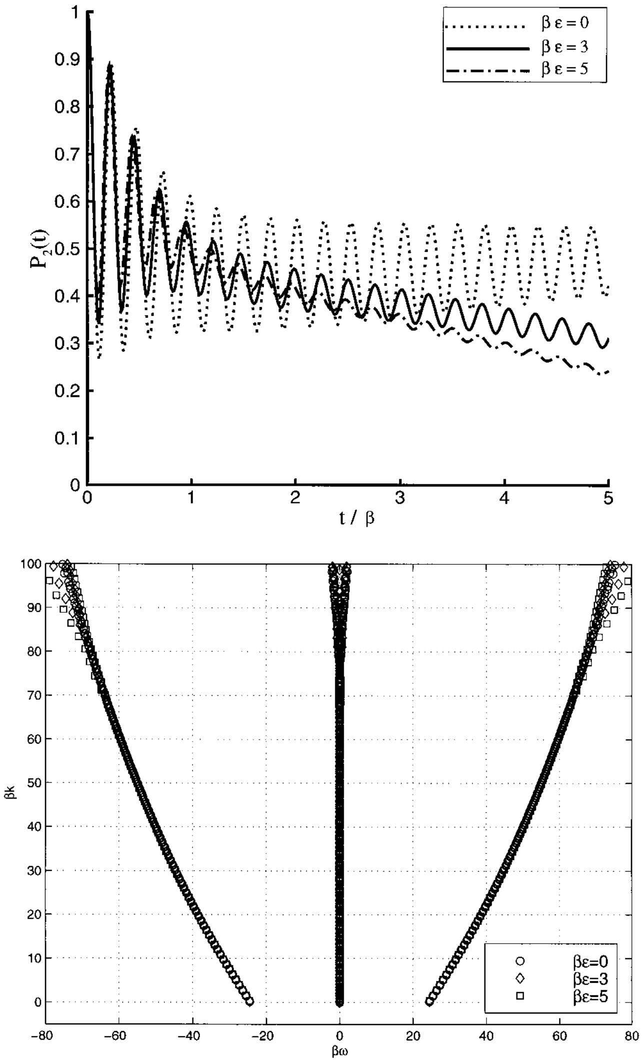

Figure 4. Comparison of (a, top) the dynamics and (b, bottom) the spectra in the mixed-valence system for three different energy biases. Except for the energy bias, all the other parameters are set equal to those used in Figure 3. Agreements between the results of numerical and spectral propagation have been checked in these cases.

IV. Concluding Remarks

In this paper we have applied the spectral analysis method to the nonadiabatic two-state diffusion equation that describes electron transfer dynamics in Debye solvents. In particular, we have examined electronic coherence in mixed-valence compounds and demonstrated that underdamped Rabi oscillations are observed in an overdamped solvent environment. Detailed study of the spectral structure of the nonadiabatic operator for various energy biases and coupling constants allows us to determine the underlying mechanisms of electron transfer kinetics. Eigenvalues form three branches in the eigendiagram: a single branch of real eigenvalues and two symmetric branches

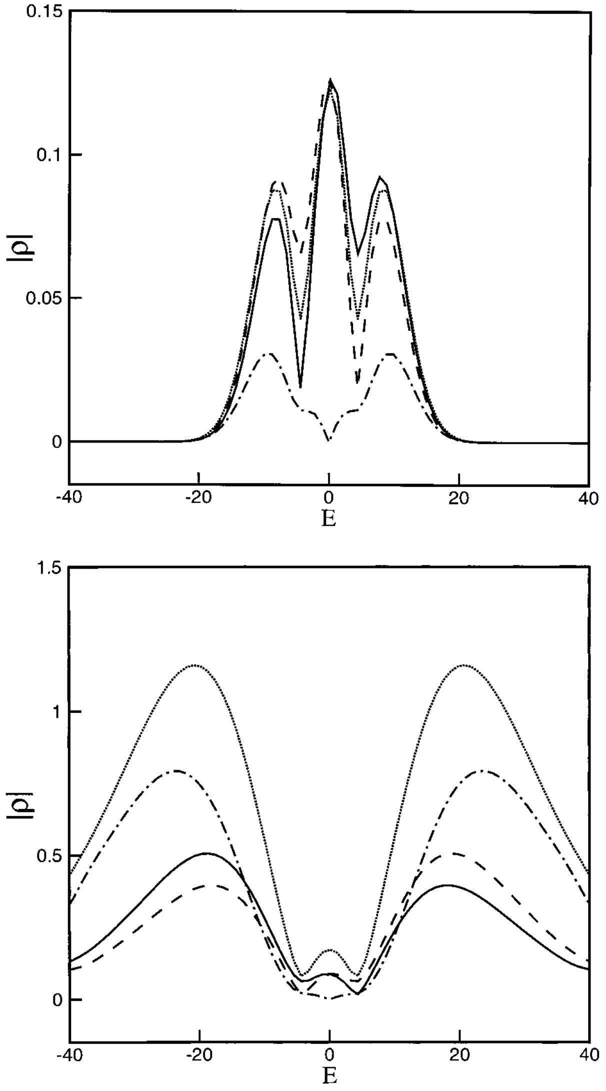

Figure 5. (a, top) Right and (b, bottom) left eigenfunctions with an eigenvalue $\beta Z = 2.6228 \pm i26.394$ for a symmetric bias case ($\beta\epsilon = 0$). All the other parameters are set equal to those used in Figure 3 except for the energy bias. Each line corresponds to ρ_1 (solid), ρ_2 (dashed), u (dot-dashed), and v (dotted), respectively.

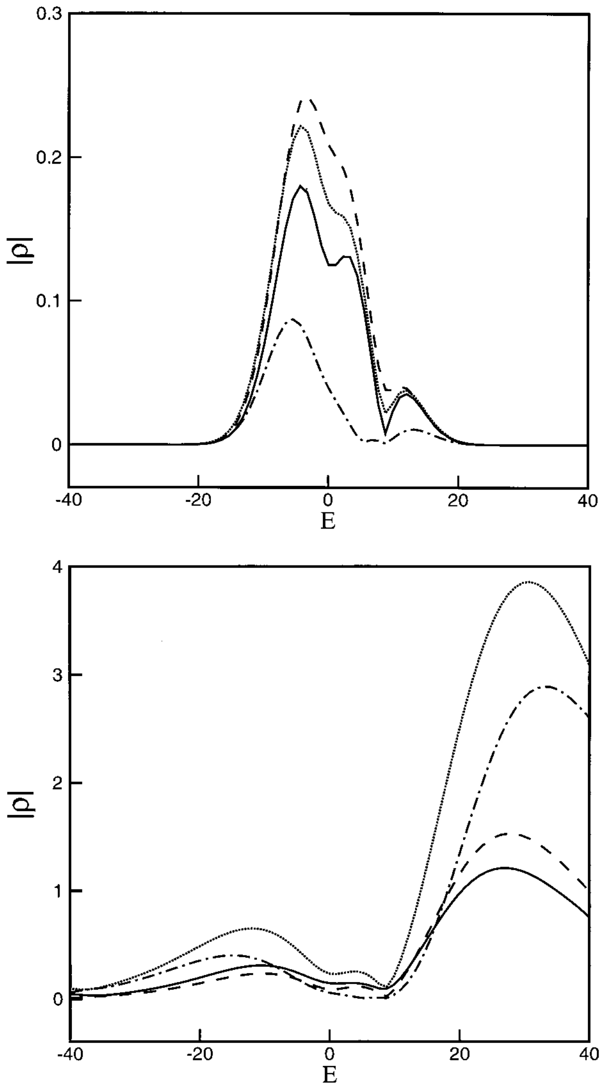

Figure 6. (a, top) Right and (b, bottom) left eigenfunctions with an eigenvalue $\beta Z = 2.8057 \pm i26.466$ for an asymmetric bias case ($\beta\epsilon = 5$). All the other parameters are set equal to those used in Figure 3 except for the energy bias. Each line corresponds to ρ_1 (solid), ρ_2 (dashed), u (dot-dashed), and v (dotted), respectively.

of complex conjugate eigenvalues. In strongly coupled systems, all three branches have a similar order of magnitude, indicating that both multiple-exponential decay and coherent oscillations can be observed experimentally.

We have investigated the dependence of the spectral structure on the coupling constant. In the very weak coupling regime, the lowest excited state is well separated from higher states, which makes the electron transfer dynamics a well-defined rate process. In the strong coupling regime, however, the eigenvalue diagram shows coalescence/bifurcation behavior in the complex plane. We have used the spectral method to calculate the time evolution of the density matrix, and indeed, observed electronic coherence in the temporal behavior of population in the acceptor state for nonequilibrium initial distributions. We also found a good agreement between results of the spectral propagation method and the numerical propagation method for small energy bias cases. Due to non-Hermitianity of the nonadiabatic operator, the spectral propagation method was not numerically stable for large energy bias cases.

For an isolated quantum system, the eigensolution to the Schrödinger equation completely determines its dynamics. In a similar fashion, the eigensolution to the nonadiabatic diffusion operator completely characterizes the dynamics of a dissipative system and thus provides a powerful tool to analyze dissipative dynamics. It is well-known that quantum dynamics comes from the underlying spectra, especially in gas-phase chemical systems;[32] however, the spectral aspect of condensed phase dissipative systems has not been well recognized yet and deserves further investigation. Though the analysis presented here is restricted to semiclassical dissipative systems, it may also be applied to quantum dissipative dynamics. In principle, we can derive the evolution equation for quantum dissipative systems either from first principles or through numerical reduction, and then pose the quantum dissipative equation of motion as an eigenvalue problem. Along this line, the dissipative dynamics of the spin−boson Hamiltonian, which has been studied mostly as a dynamic problem,[6,33] can also be explored as a spectral problem in the future.

Acknowledgment. The authors thank the NSF for financial support. J.C. thanks the MIT start-up fund and the Petroleum Research Fund for financial support. Y.J. thanks the Korean Foundations for Advanced Studies for financial support.

References and Notes

(1) Vos, M. H.; Rappaport, F.; Lambry, J.-C.; Breton, J.; Martin, J.-L. *Nature* **1993**, *363*, 320.

(2) Jonas, D.; Bradford, S.; Passino, S.; Fleming, G. *J. Chem. Phys.* **1995**, *99*, 2554.

(3) Arnett, D. C.; Vohringer, P.; Scherer, N. F. *J. Am. Chem. Soc.* **1995**, *117*, 12262.

(4) Reid, P. J.; Silva, C.; Barbara, P. F.; Karki, L.; Hupp, J. T. *J. Phys. Chem.* **1995**, *99*, 2609.

(5) Lucke, A.; Mak, C. H.; Egger, R.; Ankerhold, J.; Stockburger, J.; Grabert, H. *J. Chem. Phys.* **1997**, *107*, 8397.

(6) Makarov, D.; Makri, N. *Chem. Phys. Lett.* **1994**, *221*, 482.

(7) Evans, D. G.; Nitzan, A.; Ratner, M. A. *J. Chem. Phys.* **1998**, *108*, 6387.

(8) Coalson, R. D.; Evans, D. G.; Nitzan, A. *J. Chem. Phys.* **1994**, *101*, 486.

(9) Cho, M.; Silbey, R. J. *J. Chem. Phys.* **1995**, *103*, 595.

(10) Harris, R. A.; Silbey, R. *J. Chem. Phys.* **1983**, *78*, 7330.

(11) Silbey, R.; Harris, R. A. *J. Chem. Phys.* **1984**, *80*, 2615.

(12) Carmeli, B.; Chandler, D. *J. Chem. Phys.* **1985**, *82*, 3401.

(13) Chandler, D. In *Liquides, Cristallisation et Transition Vitreuse, Les Houches, Session LI*; Levesque, D., Hansen, J., Zinn-Justin, J., Eds.; Elsevier: New York, 1991.

(14) Leggett, A. J.; Chakravarty, S.; Dorsey, A. T.; Fisher, M. P. A.; Garg, A.; Zwerger, W. *Rev. Mod. Phys.* **1987**, *59*, 1.

(15) Marcus, R. A.; Sutin, N. *Biochim. Biophys. Acta.* **1985**, *811*, 265.

(16) Newton, M. D.; Sutin, N. *Annu. Rev. Phys. Chem.* **1984**, *35*, 437.

(17) Bader, J. S.; Kuharski, R. A.; Chandler, D. *J. Chem. Phys.* **1990**, *93*, 230.

(18) Cao, J. *Chem. Phys. Lett.*, in press.

(19) Cao, J. *J. Chem. Phys.*, in press.

(20) Zusman, L. D. *Chem. Phys.* **1980**, *49*, 295.

(21) Calef, D. F.; Wolynes, P. G. *J. Phys. Chem.* **1983**, *87*, 3387.

(22) Hynes, J. T. *J. Phys. Chem.* **1986**, *90*, 3701.

(23) Garg, A.; Onuchic, J. N.; Ambegaokar, V. *J. Chem. Phys.* **1985**, *83*, 4491.

(24) Sparpaglione, M.; Mukamel, S. *J. Chem. Phys.* **1988**, *88*, 3263.

(25) Cao, J.; Voth, G. A. *J. Chem. Phys.* **1997**, *106*, 1769.

(26) Onuchic, J. N.; Wolynes, P. G. *J. Chem. Phys.* **1993**, *98*, 2218.

(27) Yang, D. Y.; Cukier, R. I. *J. Chem. Phys.* **1989**, *91*, 281.

(28) Simons, J. *Chem. Phys.* **1973**, *2*, 27.

(29) Risken, H. *The Fokker-Planck Equation*; Springer-Verlag: New York, 1984.

(30) Dahmen, K. A.; Nelson, D. R.; Shnerb, N. M. *cond-mat/9903276* **1999**.

(31) Press, W. H.; Teukolsky, S. A.; Vetterling, W. T.; Flannery, B. P. *Numerical Recipes in FORTRAN*, 2nd ed.; Cambridge University Press: Cambridge, U.K., 1992.

(32) Field, R. W.; O'Brien, J. P.; Jacobson, M. P.; Solina, S. A. B.; Pollik, W. F.; Ishikawa, H. *Adv. Chem. Phys.* **1997**, *101*, 463−490.

(33) Wang, H.; Song, X.; Chandler, D.; Miller, W. H. *J. Chem. Phys.* **1999**, *110*(10), 4828.